Supplementary information I: Simulation Data Generation for Network Training

Data generation for network training employed our digital twin system to produce realistic, high-fidelity paired dose and acoustic datasets. We first extracted 75 unique pencil-beam dose maps—50 from a prostate patient plan and 25 from a liver patient plan—and partitioned them into training (30 prostate, 15 liver), validation (10 prostate, 5 liver), and test (10 prostate, 5 liver) cohorts to ensure robust model training and evaluation.

To emulate clinical variability and bolster model robustness, each beam underwent systematic spatial augmentation along two orthogonal axes. Axial offsets from the virtual transducer were applied in 1 cm increments spanning 4 cm to 8 cm—mimicking different depths of origin within the patient anatomy—while lateral displacements of ±1 cm in the superior, inferior, left, and right directions (plus the unshifted central position) simulated realistic setup and positioning errors. The resulting 5 × 5 grid of depth and off-center shifts generated 25 distinct variants per beam, yielding 1,875 total instances without compromising the underlying physical fidelity of the simulations.

Each dose map was first cropped to a 64 mm × 64 mm × 96 mm volume at 1 mm isotropic resolution and then fed into the digital twin simulation system as initial pressure distribution to generate its corresponding time-domain sinogram and time-reversal (TR) reconstruction. The resulting pressure field, raw sinogram, and TR reconstruction were then grouped into triplets and supplied to the network as training samples.

Supplementary information II: FLASH Electron Transfer Learinig

The FLASH electron experiments were conducted using six different collimators to introduce variability in the experimental setup. Each experiment resulted in only six sinograms, which posed a challenge in terms of dataset size. To overcome this limitation, we applied a data augmentation strategy by utilizing a digital twin model. In this model, the electron pulse was integrated into the simulation pipeline as shown in Supplementary Figure 1 b).

The simulated data generated through the digital twin model included variations in both depth and translation locations. Specifically, five different depths (ranging from 3 to 7 cm) were simulated, along with five different translation positions (center, up, down, left, and right). This resulted in a total of 150 distinct datasets, significantly enhancing the diversity of the training data.

The PINN model, initially trained on proton data, had already learned the fundamental principles of limited-view enhancement. Consequently, the trained proton PINN model was transferred to the electron dataset. The electron-specific training data were then used to fine-tune the model, leveraging the existing knowledge from the proton dataset to enhance the reconstruction quality for the FLASH electron experiments.

For model tuning, four collimators were used to train the deep learning models, while one collimator was reserved for validation, and the remaining one was used for testing. This dataset configuration ensured that the models were trained on a representative range of experimental conditions while preserving the integrity of the validation and testing phases.

Supplementary information III: Network Training Details

The grouped triplets were input into the network for training. Initially, the time-reversal (TR) reconstructions and the corresponding pressure distributions were used to train the model. The trained network was then employed to generate predicted pressure maps, which were subsequently input into the forward simulation module to produce predicted sinograms. However, the forward simulation process takes approximately 3 seconds per volume, meaning that one full iteration for the entire dataset would take around 1 hour. To reduce the training time, we implemented a strategy where, during the forward operation, only one volume per unique beam was randomly selected to generate a predicted sinogram. This approach allowed us to compare the predicted sinogram with the ground truth sinogram and compute the loss between them, effectively reducing the number of volumes used for the forward simulation to 60 per iteration.

Additionally, during the early training stages, the difference between sinograms was much smaller than the difference between pressure maps, so we opted to run the forward simulation only after every five consecutive epochs, thus reducing the total number of forward simulations by a factor of five. The network training was performed using Keras2 in Python 3.7, with training conducted on an RTX A6000 GPU. The loss functions for both $\mathcal{L}_p$ and $\mathcal{L}_s$ were using 'reduce_mean' functions. The weighting parameters λ_1 and λ_2 were arbitrarily set to 0.8 and 0.2, respectively, to balance the two loss components and optimize the training process. Moreover, when the value of $\lambda_2\mathcal{L}_S$ is larger than $\lambda_1\mathcal{L}_p$, the forward simulation was performed after each epoch.

Supplementary Information IV: Dose Calibration

The MEVION system delivers a standard pulse of 8 pC (verified by machine log files), and from our routine machine QA we determined a conversion of 14.5 pC per MU, which implies each pulse corresponds to 0.55 MU. In our water-tank calibration, we prescribed 100 MU, yielding 311 cGy at the Bragg-peak reference depth (7 cm from the transducer array). These values establish the baseline relationship between delivered charge, machine-reported MU, and absolute dose in a controlled geometry.

When performing reconstruction, we always use sinograms that contain an integer multiple of 100 pulses. From the parameters above, each pulse corresponds to 1.71 cGy, so 100 pulses deliver 171 cGy. This "100-pulse" unit simplifies the pressure-to-dose scaling in our PINN reconstructions and ensures consistency across datasets.

In principle, the dose in the human phantom, D_h, can be obtained by scaling the water-tank calibration factor K according to the ratio of Grüneisen parameters and densities:

$$D_h = K(\frac{\Gamma_w \rho_w}{\Gamma_h \rho_h}) p_h$$

where p_h is the reconstructed pressure map in the human torso phantom, Γ_w, ρ_w are the Grüneisen parameter and density of water, and Γ_h, ρ_h are those of the phantom. However, because the absolute Grüneisen parameter Γ_h of our human phantom is unknown, the factor $\frac{\Gamma_w \rho_w}{\Gamma_h \rho_h}$ cannot be determined, and direct conversion to D_h is therefore inaccessible.

To work around this limitation, we generated the phantom treatment plan under the same criteria as the water-tank experiment. Specifically, we again prescribed 100 MU and matched the beam setup to place the Bragg-peak at 5.2 cm from the transducer array in the phantom geometry. By replicating the reference conditions, the system response at the phantom Bragg-peak remains consistent with the water-tank calibration, enabling us to extract an effective, comparative calibration factor for dose reconstruction in the torso phantom.

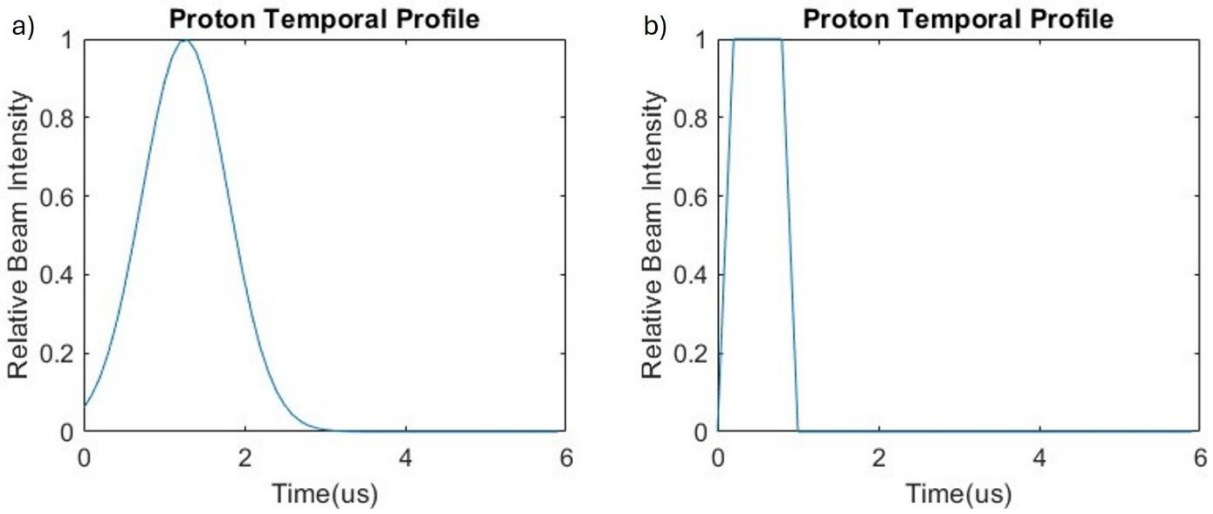

SF 1. Temporal profiles for the radiation source. a) The generated temporal profile for the proton pulse from MEVION machine. Originally measured using a scintillator-photodiode. b) The temporal profile for the FLASH electron pulse from MOBETRON machine. Originally measured from the beam-current transformer (BCT).

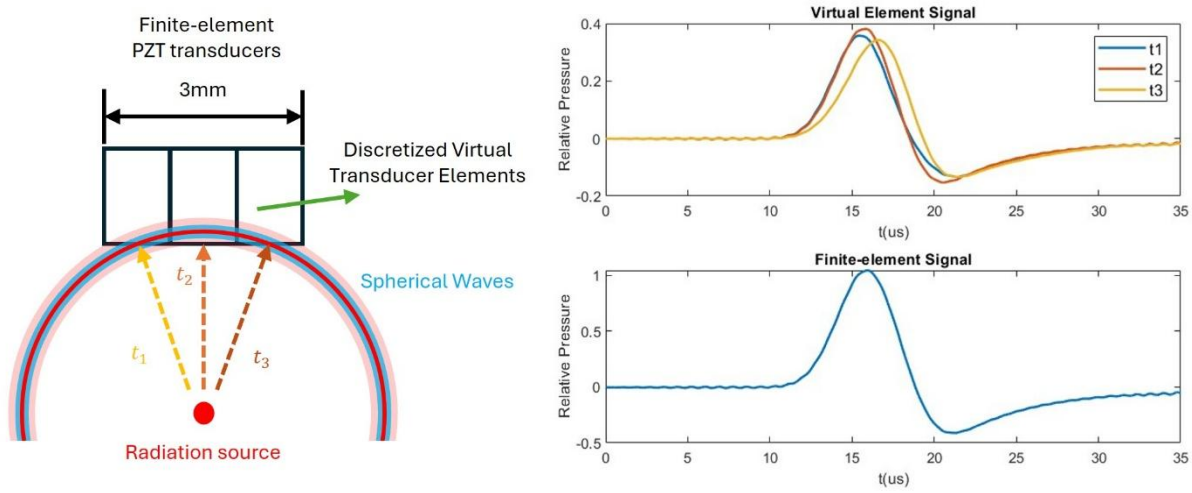

SF 2. Demonstration of qRAI detection through finite transducer elements. a) The radiation source created spherically propagated acoustic waves. The 3mm piezoelectric transducer elements can be discretized into 3 virtual elements. Each element receives the signal at different time t_1, t_2, and t_3. All three signals are summed together to form the final measured signals. b) The received signals at different time t_1, t_2, and t_3 and the summed finite-element signal.

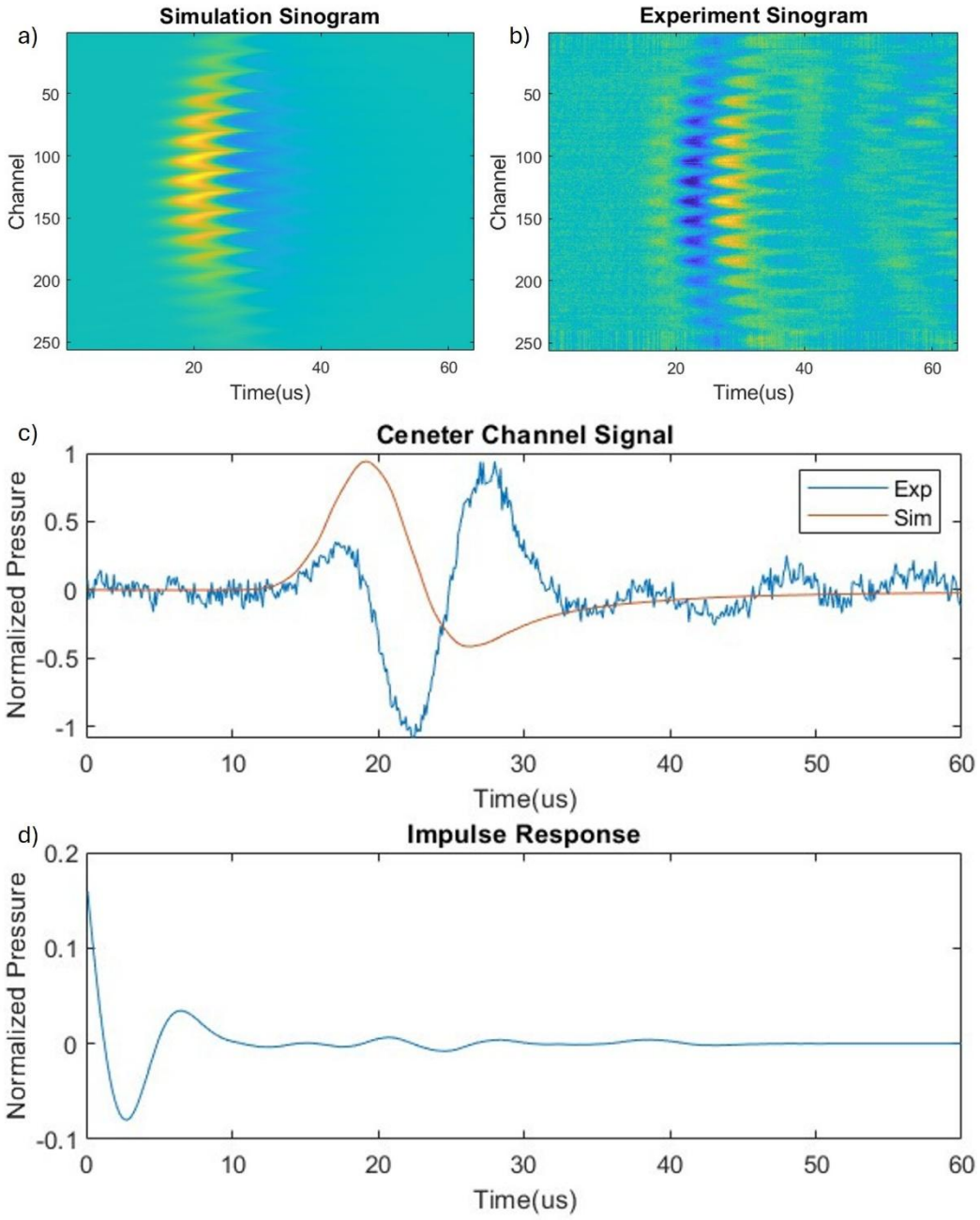

SF 3. Process of impulse response calibration. a) The simulation sinogram that integrated the proton pulse duration and the transducer finite-element effect. b) The water tank experimental sinogram measured with exactly same setup as the simulation. c) Comparison of the center (120th) channel's signal between the simulation sinogram and the experimental sinogram. d) The result of the deconvoluted impulse response for the planar array transducer.

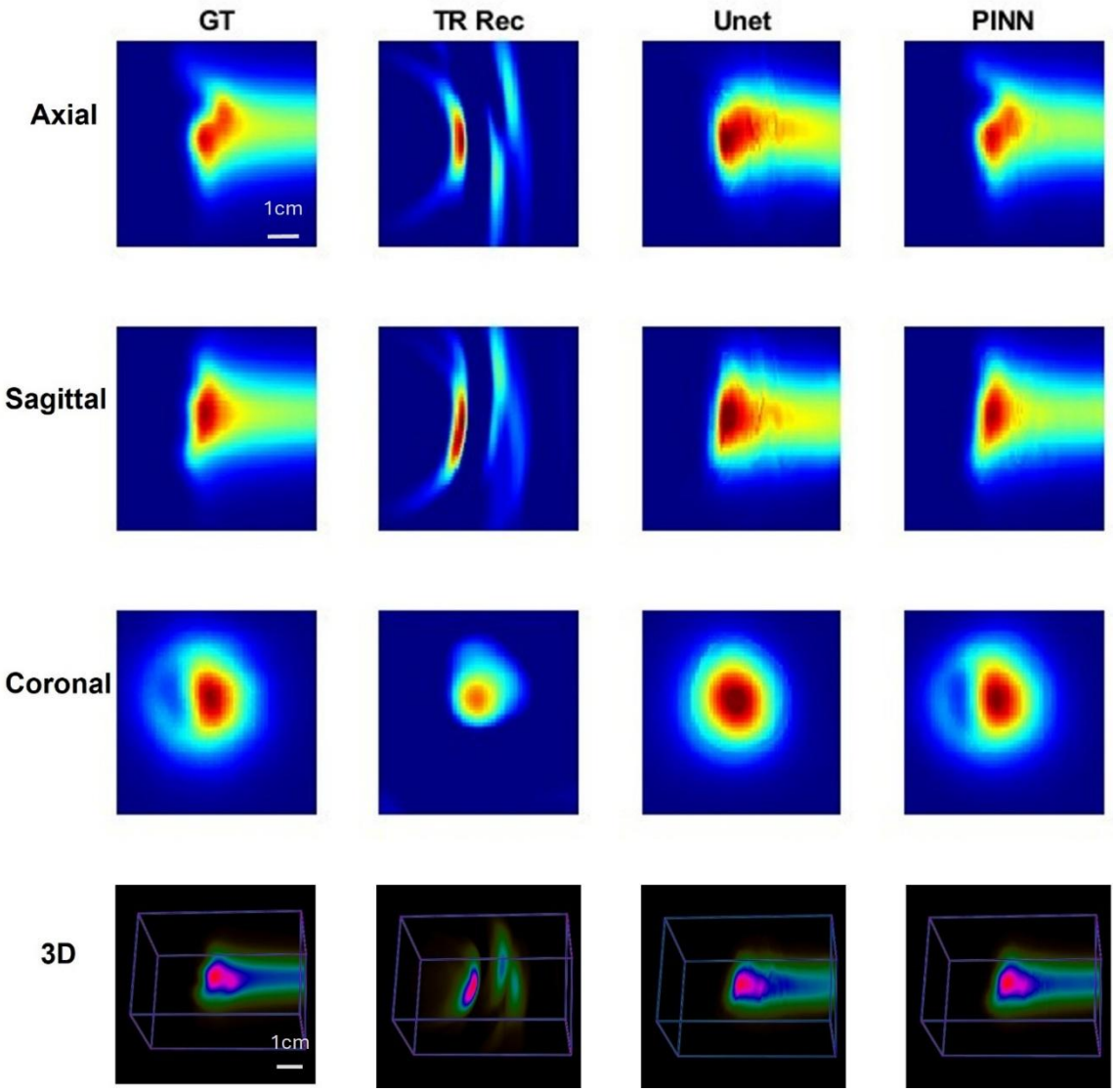

SF4. Simulation Results. This figure presents a comparison of the ground truth (GT, first column), time-reversal reconstruction (TR Rec, second column), U-Net enhancement (third column), and PINN enhancement (fourth column) across four views: axial view (first row), sagittal view (second row), coronal view (third row), and 3D view (fourth row). The GT is extracted from a prostate patient's dose map generated from RayStation. The TR Rec is obtained through time-reversal reconstruction alone. Both U-Net and PINN enhancements are trained with the digital twin simulated dataset with 75 unique pencil beams.

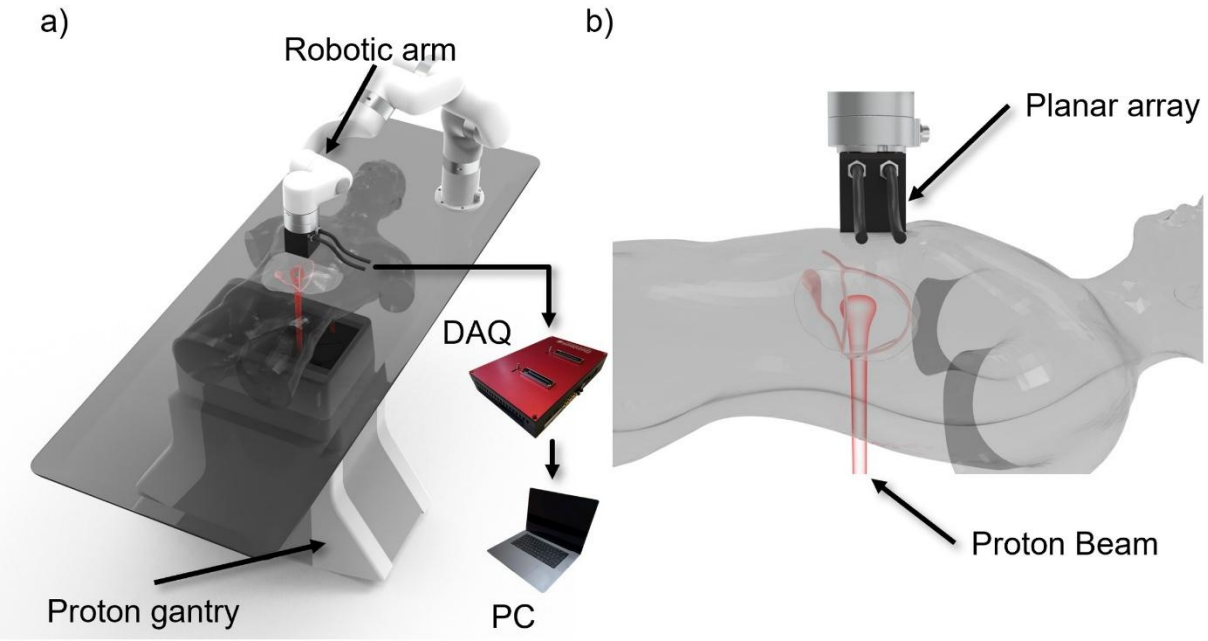

SF 5. The setup demonstration for the proton experiments which takes the real treatment scenario into consideration. a) The human-torso phantom is positioned on the couch. The planar array is pressed on to the patient by a robotic arm and is connected to a data acquisition (DAQ) system controlled by an external computer. The proton beam is delivered from below the patient. a) The side view of the qRAI measurement during the liver treatment.

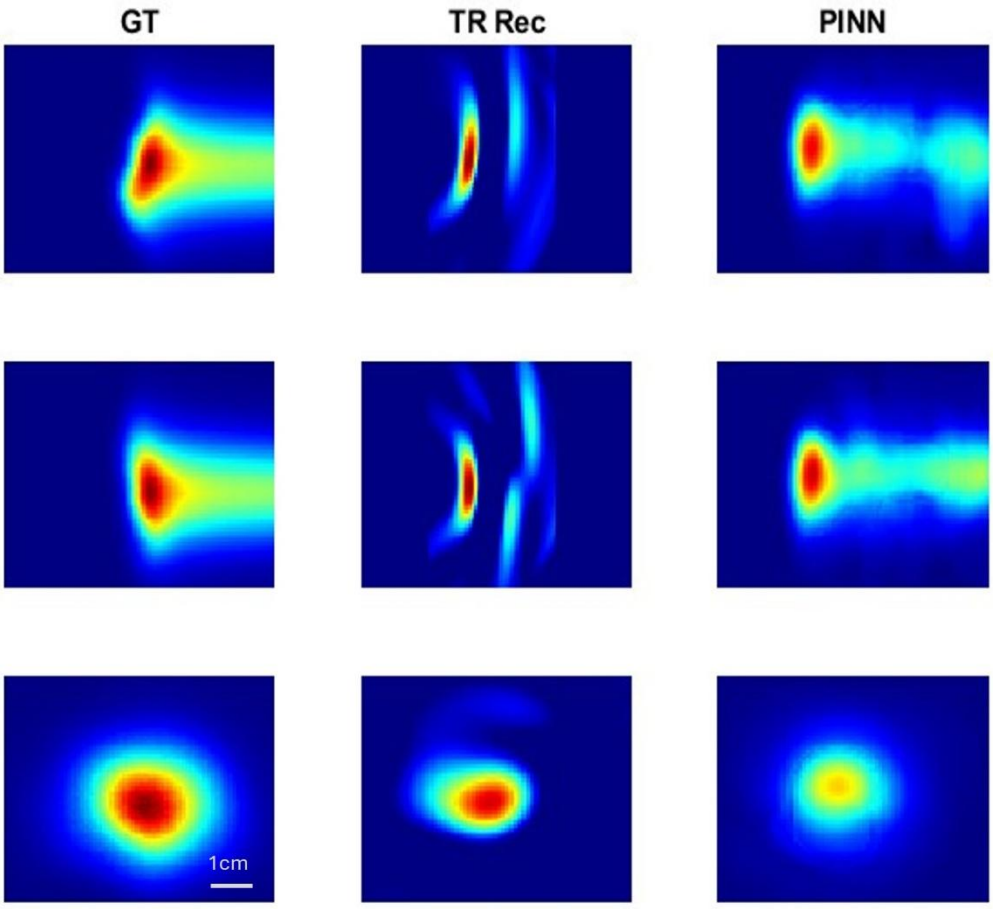

SF6. Tuning Results. This figure presents a comparison of the ground truth (GT, first column), time-reversal reconstruction (TR Rec, second column), and tuned-PINN enhancement (third column) across four views: axial view (first row), sagittal view (second row), and coronal view (third row). The network tends to enhance the beam to uniform water tank data because of overfitting.

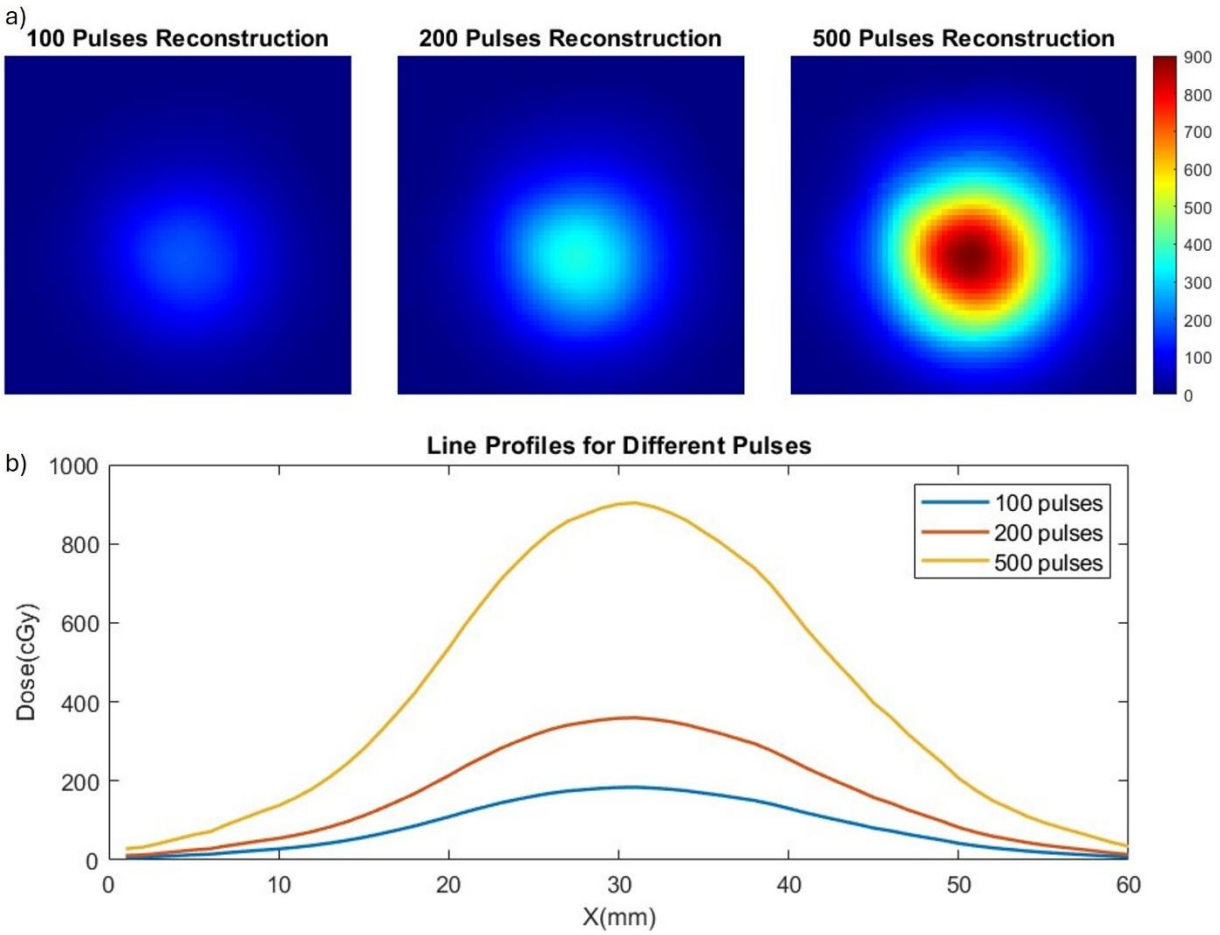

SF 7. Dose reconstruction for different pulse numbers. a) Three different reconstruction results from the sinogram measured by accumulating 100, 200, and 500 proton pulses individually. b) The line profiles comparison at the Bragg Peak, showing the intensity changes of the reconstruction.

Type of Tissue	Sound Velocity [m/s]	Density [g/cm^3]	Attenuation coefficient [dB/cm/MHz]
Organs with Speckles (liver, kidneys, etc.)	1400±10	0.99	0.5±0.1
Organs without Speckles (stomach, intestines, etc.)	1400±10	0.99	0.5±0.1
Body Tissue	1400±10	1.00	0.6±0.1
Cortical Bone	3000±30	2.31	3.2±0.2
Trabecular Bone	2800±50	2.03	10±1

Supplementary table 1. Human phantom parameters.

	TR	**UNET**	**PINN**
SSIM	0.396±0.022	0.956±0.009	0.985±0.007
PSNR	16.24±0.58	36.01±1.16	40.53±1.66
GI: 3mm/3%	0.104±0.010	0.971±0.018	0.988±0.012

Supplementary table 2. Quantitative analysis for the simulation results.